Graphene Oxide Decorated with Nickel Cobaltite Nanoparticles as an Adsorbent for Cationic Methyl Green Dye: Kinetic, Isotherm, and Thermodynamic Studies

Maryam Abdulsatar Abduljabar 🆔 ✉, *Sundus Hadi Merza** 🆔 ✉

Department of Chemistry, College of Education for Pure Sciences (Ibn Al-Haitham), University of Baghdad, Baghdad, Iraq.
*Corresponding Author.

Abstract

In this study, graphene oxide (GO) flakes were embellished with $NiCo_2O_4$ (NC) nanoparticles by in situ deposition, and the produced composite (NC: GO) was utilized as an adsorbent to remove methyl green dye (MG) from aqueous solutions. The successful coating of graphene oxide with nickel cobaltite nanoparticles (NC) was verified using FT-IR, SEM and X-ray diffraction (XRD) studies. The crystalline particle sizes of NC nanoparticles and NC nanoparticles decorated GO were 10.53 nm and 9.30 nm respectively. The impact of several experimental factors, including time of contact, the dosage of adsorbent, and temperature were investigated. The optimal contact time and adsorbent dosage were 120 minutes and 3 mg/L, respectively. The adsorption data fitted better to Freundlich isotherm. Four kinetic models were used to track the adsorption process: a pseudo first-order equation, a pseudo second-order equation, an intraparticle diffusion equation, and the Boyd equation. Modeling of the experimental data revealed that the adsorption kinetics was well represented by the pseudo-second order model(R^2=0.9945) with a rate constant of 3.2×10^{-3} (g/mg. min). MG dye is gradually absorbed by the NC nanoparticles through intraparticle diffusion and is afterward held in smaller pores. The values of the thermodynamic analysis showed that the MG dye adsorption was an endothermic in nature, spontaneous and phyisorption process.

Keywords: Boyd equation, Debye-Scherer equation, Intraparticle diffusion, Interplanar spacing, Pseudo first order model.

Introduction

Given the increased rate of pollution and depletion of natural resources, researchers and environmentalists are concerned about water contamination because of its negative effects on the ecosystem. Water can contain a variety of pollutants, including heavy metals, organic compounds, chemical waste, and dyes. Dyes are categorized as significant pollutants on humans and the environment. Many of them have a history of causing cancer or being toxic[1]. Dye degradation is more challenging due to their xenobiotic characteristics, resistance to a variety of chemicals and oxidizing agents, and complicated aromatic structures[2]. To treat dye-containing wastewater diverse techniques can be used, such as membrane filtration[3],coagulation, nano-filtration and flocculation[4], reverse and forward osmosis[5], biological treatments[6], nano-photocatalyst and

advanced oxidative processes[7,8]. However, several of these techniques have certain setbacks and are expensive and energy-intensive. Adsorption is still one of the best treatment alternatives due to its simplicity, ease of use, and low cost in contrast to other approaches.

Nano-adsorbents including oxides of transitional elements like Mn, Fe, Co, and Ni [9-12], bimetallic oxide[13] and graphene and its derivative[14-16] are frequently used in the removal of various pollutants because of their roles in the adsorption process. Graphene oxide, one of the two-dimensional structures of carbon allotropes, is synthesized by chemically oxidizing the graphite layers. GO are widely used in wastewater treatment due to its large surface area, high water dispersibility, high mechanical strength, and decorated with reactive functional groups on the basal plane and the edge[17]. Similarly, bimetallic oxides, cobaltite in particular, which has the general formula MCo_2O_4 (M = Zn, Mn, Cu, Fe, Ni, or Mg), has been suggested as a potential material to consider for adsorption performance due to its electrical and magnetic properties, availability in nature, low cost, less toxic, and environmentally friendly [18–20,13].

The major goal of this work is to immobilize nickel cobaltite NC nanoparticles on the surface of GO and use it as a non-toxic adsorbent. A sol-gel approach was used to generate the nickel cobaltite-graphene oxide (NC: GO) nanocomposite, which then underwent calcination and demonstrated adsorption performance toward the methyl green (MG) dye. MG is a dicationic triphenylmethane that is commonly used in biology and medicine to change the color of solutions as well as a photochromophore to ignite coagulated films. The experiment was conducted based on the kinetic, isothermal, and thermodynamic properties as well as the variables that affect adsorption, such as temperature and adsorbent dosage. NC: GO nanocomposite was characterized by FT-IR and XRD techniques.

Materials and Methods

Graphite powder with an average size of 75 μm was purchased from Fluka. H_2SO_4 (98%), H_2O_2 (30%), $NaNO_3$, and $KMnO_4$ were supplied by Merck. HCl and NaOH were purchased from GCC Company. Co $(NO_3)_2 \cdot 6H_2O$ and Ni $(NO_3)_2 \cdot 6H_2O$ were supplied by BDH. Methyl green (MG) (Molecular Weight 458.47: chemical formula: $C_{26}H_{33}Cl_2N_3$; maximum wavelength (λ_{max} =618 nm) supplied by win lab limited-United Kingdom, was used without further purification. The structural investigation and the average size of the prepared materials were studied by X–ray powder diffractometer (XRD),6000 Shimadzu (Japan) profiles were registered using Cu (1.54060), Voltage: 40.0 kV and Current: 30.0 mA. The features of functional groups were examined by the FT–IR spectra on the Shimadzu, 8400s, (Japan) spectrophotometer.

Fabrication of Graphite Oxide (GTO) and Nickel Cobaltite- graphene Oxide

Nanocomposite (NC: GO)

The GTO was synthesized using Hummer method [21, 22] .A mixture of 10 g graphite and 5 g sodium nitrate was mixed vigorously with 230 mL of 98% sulphuric acid in an ice bath for half an hour. Then 30 g of potassium permanganate was added carefully and stepwise to prevent the temperature exceeding 20 °C.

After that, the ice bath was removed and the temperature brought to 35 ± 3 °C and maintained for half an hour. The second step involved adding 460 mL of water to raise the temperature to 98 °C for 15 minutes. The color suspension was brown. The suspension was further diluted with 1400 mL of warm water. The colorless soluble manganese sulphate was obtained by treating the suspension with 30% hydrogen peroxide. Finally, the warm suspension was filtered and washed with 5% HCl solution and then with distilled water until pH reached 7. The obtained filter cake was dried in a vacuum oven for 48 hours. In the subsequent process, NC nanoparticles were in situ deposited on GO flakes. Firstly 0.05 g of GTO was dispersed in 10 mL distilled water using a probe ultrasonic for 1 hour. Then added slowly to a mixture of the same types and molarity solutions of Ni $(NO_3)_2.6H_2O$ and Co $(NO_3)_2.6H_2O$. The mixture's pH was raised to 9 gradually by adding 50 mL of 0.75 M NaOH under vigorous stirring. The temperature maintained between 50 – 60 °C. The formed gel was collected by centrifugation, washed, dried at 100 °C, and finally calcined at 300 °C for 2 hours. The resulting nanocomposite was denoted as NC: GO.

Calibration Curve of MG Dye

Prior to the adsorption procedure, standard solutions in the range of 1–15 mg/L were prepared daily by serial dilution from the MG stock solution, which was prepared by dissolving 0.1 g in 1000 ml of distilled water. The absorption was assessed using a UV-visible spectrophotometer at λ_{max} =618 nm. The calibration curve was created using the Beer-Lambert law by plotting the absorption results against the standard dye solution concentration. The determined slope served as a guide for determining concentration in the remaining experiments. Fig. 1 displays the calibration curve.
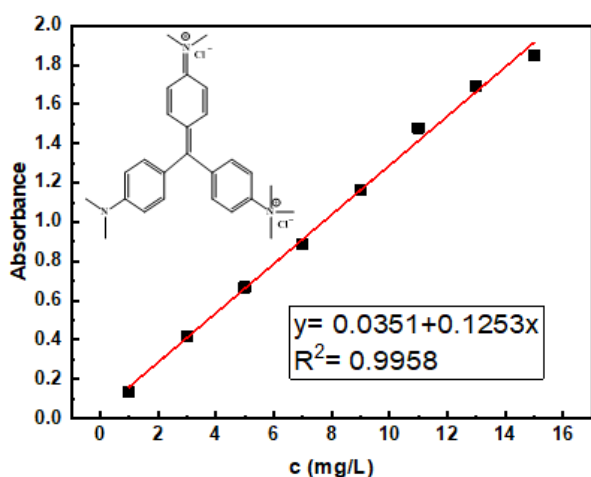

y= 0.0351+0.1253x
R^2= 0.9958

Figure 1. Calibration curve of MG dye solution.

Adsorption Experiments

The adsorption experiments were carried out in a thermostatic shaking water bath with varying temperatures of 15, 25, and 35 °C and a constant rotational speed of 120 rpm. To identify the influence of NC: GO dosage on MG dye adsorption, different amounts of adsorbent NC: GO ranging from 1 mg to 4.5 mg (0.5 mg intervals) were introduced into 10 mL of fixed initial concentration of MG solution at 25 °C until the equilibrium time was reached. The adsorption process to reach equilibrium was studied, and 10 mL of MG aqueous solution was mixed with 3 mg of the adsorbent (NC: GO) at different periods (5 to 180 minutes). The initial MG concentration was 15 mg/L. The supernatant solution and adsorbent were separated by centrifugation at 5000 rpm for 10 minutes. The quantity of MG adsorbed onto NC: GO was calculated using the following Eq. 1.

$$q_t = \frac{V\,(c_o - c_t)}{m} \qquad \ldots\ldots\ldots\ldots 1$$

Where c_o and c_t are the initial concentration and concentration at (t) time respectively, q_t is the amount of adsorbate MG (mg/g) at t time, V volume of MG dye solution (L), and m weight of adsorbent (g). To examine the impact of temperature, the temperature was held at a different range of temperatures (15– 25– 35 °C) with varying concentrations of MG dye. The amount of MG adsorption at equilibrium q_e (mg/g) was calculated using the above equation where $q_t = q_e$ and $c_t = c_e$. A spectrophotometric approach was used to measure the remaining final MG concentrations in the solution at a maximum wavelength λ_{max} of 618 nm.

Results and Discussion

Characterization

The XRD diffractogram of (GO), NC undoped, and NC doped with GO (NC: GO) are shown in Fig. 2. XRD patterns of GO show distinct diffraction peaks at 10.08 (d= 8.76 nm), the increasing interlayer space of GO, and the formation of a broad graphitic peak with lower intensity indicates intercalated many oxygen functional groups within the graphite Lattice. NC characteristic peaks and JCPDS (card no. 073-1702) are in good agreement [23]. The matching in (d) and the small displacement change in (2θ) support the preparation of NC. Table 1 lists the prepared NC and the JCPDS interplanar spacing (d) and diffraction peak positions (2θ). The pattern of the nanocomposite (NC: GO) exhibits the same peaks

that are attributed to NC. No peaks of GO were seen, which indicates that NC nanoparticles are coating the surface of GO nanosheets, or, to put it another way, that NC has virtually completely covered the GO surface.

Table 1. The interplanar spacing (d) and diffraction peak positions of NiCo₂O₄ compared with JCPDS (card no. 073-1702 and 00-020-0781).

Mille index	(2θ) degree		(d) spacing	
	NiCo₂O₄ prepared	JCPDS (073-1702)	NiCo₂O₄ prepared	JCPDS (073-1702)
(111)ᵃ	19.145°	18.928°	4.63	-
(220)	31.261°	31.152°	2.85	2.87
(311)	36.849°	36.705°	2.43	2.45

(400)	44.792°	44.635°	2.02	2.03
(422) b	55.066°	44.635°	1.65	-
(511)	59.231°	59.115°	1.55	1.56
(440)	65.022°	64.963°	1.43	1.43
a (4.69) b (1.65) JCPDS (card no.) 00-020-0781[24]				

Using the Debye-Scherer equation shown below [25], the average crystallite size (d) in nanometers of the NC nanoparticles and NC: GO were determined.

$$d = \frac{0.94\,\lambda}{\beta_D\,cos\theta} \qquad \dots\dots\dots\dots 2$$

Where λ is the X-ray wavelength of Cu -K_α =0.1542 nm, the diffraction peak's full width at half maximum (FWHM) is β_D in radians, and the Bragg diffraction angle peak is θ. The calculated average crystallite size of NC and NC on the GO surface is 10.53 nm and 9.30 nm respectively. The reduction in crystallite size demonstrated that the inclusion of nanoparticles prevents the restacking of the GO layers in the composite and also minimizes particle agglomeration.
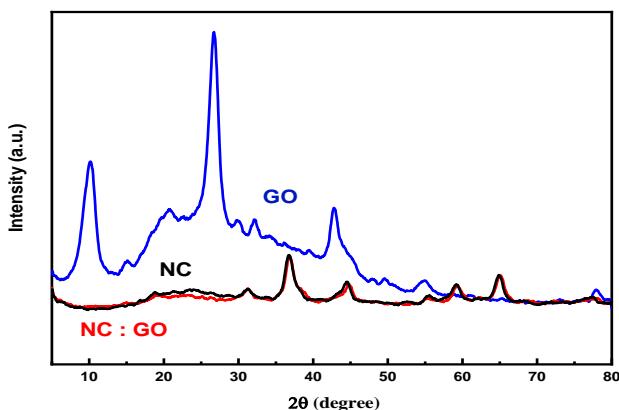

Figure 2. XRD diffractogram of the GO, NiCo$_2$O$_4$ (NC undoped), and NiCo$_2$O$_4$ doped with GO (NC: GO)

The FT-IR spectra of GO, NC, and NC: GO nanocomposite are displayed in Fig. 3. The stretching vibration at 1744 cm^{-1} is related to the C=O at the edge of GO sheets. Peaks at 1279 and 1073 cm^{-1} are associated to C-O stretching in epoxy groups[26], while peaks at 1619 cm^{-1} and 1457 cm^{-1} are related to C=C stretching of aromatic rings [27]. 1153 cm^{-1} and 712 cm^{-1} attributed to stretching of tertiary OH and OH out of plane respectively[28]. The H-O-H bending vibration mode of NC indicated by the bands at 1508 cm^{-1} and 1371 cm^{-1}. The weak bands at 662 cm^{-1} and 550 cm^{-1} were attributed to the stretching vibration of the Ni–O and Co–O, which were moved to 557 cm^{-1} and 655 cm^{-1} as in the case of NC: GO

nanocomposite [29]. The wide band between 2500 and 3500 cm^{-1} caused by O-H stretching. The FT-IR fingerprints for both the NC and GO are present in the spectrum of the NC: GO nanocomposite, further supporting the composite's formation.
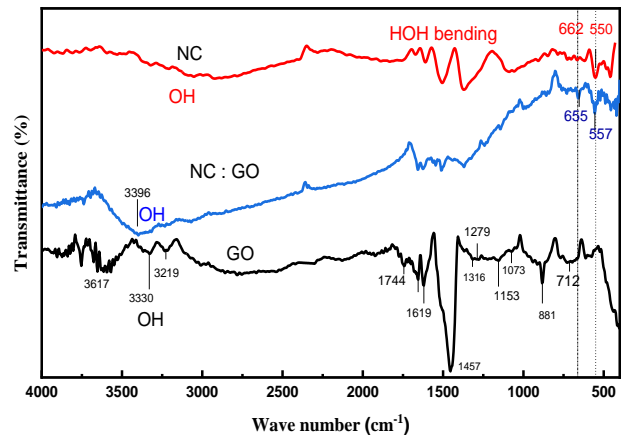

Figure 3. FT-IR spectra of NC, GO and NC: GO nanocomposite

Fig. 4 display two SEM images of the NC: GO at 35 kx and 70 kx magnification with Energy Dispersive X-Ray (EDX) analysis. The figures show that NC nanoparticles appear as a nanoplate with aggregation and an uneven distribution. The EDX of the NC: GO nanocomposite revealed the presence of carbon (C), oxygen (O), and nickel (Ni) in addition to cobalt (Co).
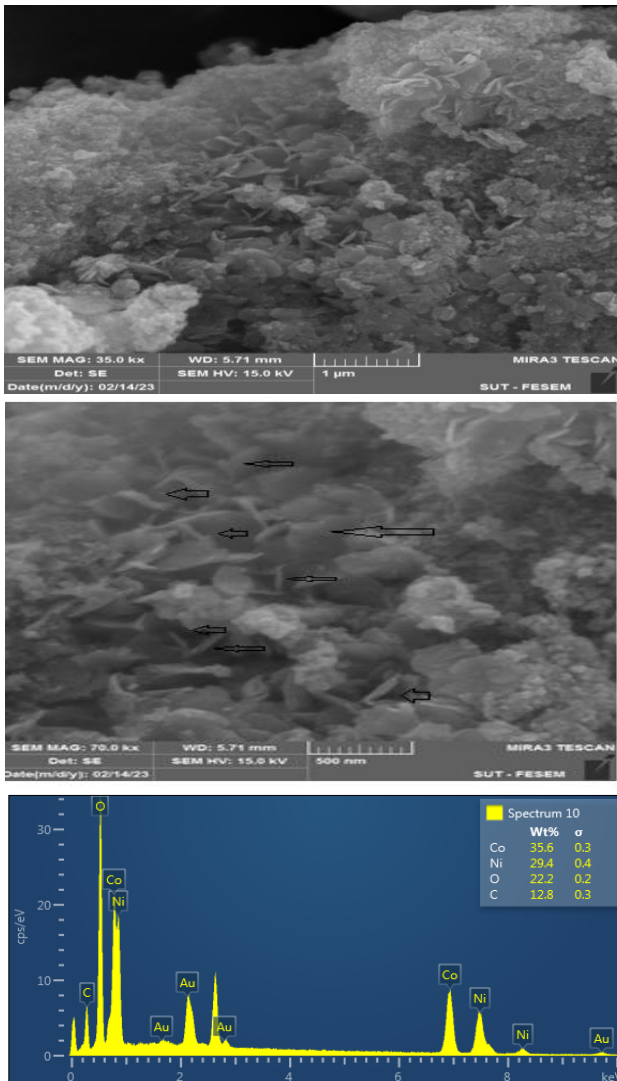
Figure 4. NC: GO nanocomposite analysis: SEM images in 35 kx , 70 kx and EDX.

Effect of Adsorbent Weight

Fig. 5 shows the impact of the adsorbent NC: GO dose on the adsorption of MG. With the increase of adsorbent weight, the percentage removal of MG increased, going from 41.7 at dose 1 mg/L to 47.59 at dose 3 mg/L. The percentage removal measurements tended to decrease with increasing dosage, the primary cause of this behavior is that during the adsorption process, adsorption sites stay unsaturated, although the number of accessible adsorption sites grows by raising the dosage of the adsorbent. The optimal and economical adsorbent dosage is 3 mg/L as shown in Fig. 5.
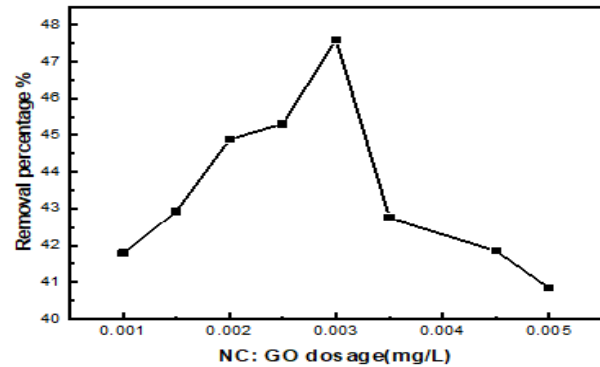

Figure 5. Effect of adsorbent dosage (NC: GO) on MG removal, (contact time 60 min, c_e= 15 mg/L)

Effect of contact time

Equilibrium time is one of the most crucial equilibrium judgment criteria for the design of wastewater treatment systems or adsorption processes. The effect of contact time 5–180 min on the adsorption capabilities of MG over NC: GO at a concentration of 15 mg/L and NC: GO dose of 3 mg/L is shown in Fig. 6. According to Fig. 6, the presence of a very high number of active sites on the adsorbent NC: GO surface may be the reason why the adsorption capacity rose quickly until the contact duration reached 60 min. A plateau reached in contact time ≥ 100 may be due to decrease in the number of surface-active sites or an increase in the repulsive forces between the MG molecules on NC: GO surface and the bulk phase [30]. Additionally, Fig. 6 demonstrates that when the temperature rises, the equilibrium adsorption capacity gradually increased, indicating that the adsorption process was preferred.
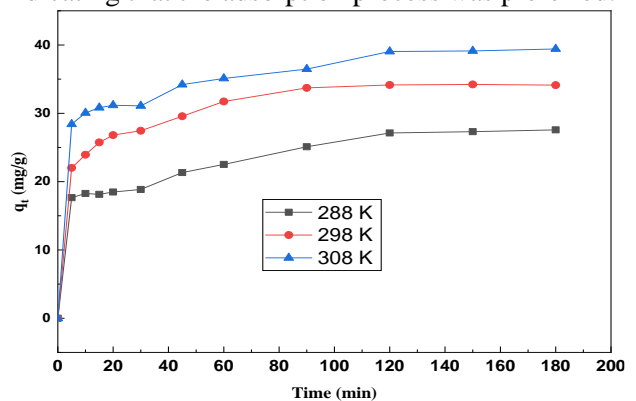

Figure 6. Contact time effect of MG adsorption on the 3 mg/10mL dose adsorbent NC: GO at different temperature

Effect of Temperature

By varying the temperatures from 288 to 308 K, the removal percentage (R%) of MG dye was determined using the following Eq. 3[31].

$$R\% = \frac{c_o - c_e}{c_o} \times 100 \qquad \text{................. 3}$$

Where the initial and equilibrium concentrations of MG are denoted by c_o and c_e, respectively. The adsorption of MG onto NC: GO nanocomposite increases as the temperature rises, as can be observed in Fig. 7. This indicates that the adsorption process is endothermic, or put another way, the MG adsorption onto NC: GO surface requires a significant amount of energy to move from the bulk solution to the surface. This behavior is the same as that of the majority of adsorption processes[32].
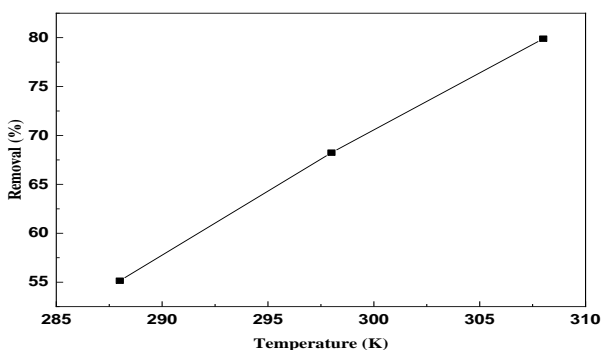

Figure 7. The temperature effect on MG adsorption onto NC: GO nanocomposite at room temperature, Initial concentration 15 mg/L.

Adsorption Kinetic Study

The kinetics of the adsorption process was investigated by conducting a series of sorption experiments at a fixed temperature and tracking the amount adsorbed over time. There are multiple steps involved in the process by which an adsorbate binds to an adsorbent at the solid-liquid interface: internal (intraparticle) and external diffusion, in which the adsorbate diffusion from and across the liquid film to the surface of solid particles: Bulk diffusion, in which the adsorbate diffusion from the bulk of the solution to the liquid film encircling the solid: and interaction of the adsorbate with the surface sites through physical or chemical bonds. The study of the kinetics of the adsorption process has led to a considerable understanding of these mechanisms. Thus, the experimental data were represented by four models: the pseudo– first order model (PFO), the pseudo– second order model (PSO), the Weber & Morris kinetic model (intraparticle diffusion ID), and

Boyd. The PFO model[32] is usefully expressed in natural logarithmic form as follows:

$$\ln(q_e - q_t) = \ln q_e - k_1 t \qquad \text{...........4}$$

Where the rate constant k_1 (1/min) and amounts of MG absorbed at equilibrium q_e (mg/g) can be found from the slope and intercept of the plot ln $(q_e - q_t)$ versus time respectively, see Fig. 8. The q_t (mg/g) represents the amounts of MG absorbed at a time (*t*) in min. The linearized forms of PSO kinetics can be defined according to Eq. 5

$$\frac{t}{q_t} = \frac{1}{k_2 q_e^2} + \frac{t}{q_e} \qquad \text{................5}$$

A plot of $\frac{t}{q_t}$ against time yields straight line then the rate constant k_2 (g/mg. min) and q_e can be calculated from the intercept and the slope respectively see Fig. 8. The kinetic parameters with the sum of squares errors (SSE) of PFO and PSO at different temperatures were obtained and summarized in Table .2.

Table 2. Parameters of the pseudo-first, second order kinetic and Weber and Morris kinetic of NC: GO towards MG dye at different temperature

	Temperature		
Pseudo-first order model	**288**	**298**	**308**
$q_{e, exp}$ **(mg/g)**	27.57	34.22	39.41
$q_{e, cal}$ **(mg/g)**	15.73	17.02	14.88
K_1(1/min)	0.0260	0.0378	0.0257
SSE	0.9474	1.5276	1.1138
R^2	0.9419	0.9549	0.9308
Pseudo-second order model			
$q_{e, cal}$ **(mg/g)**	28.90	35.46	40.32
K_2(g/mg· min)	0.0032	0.0047	0.0042
SSE	0.2442	0.0254	0.0410
R^2	0.9945	0.9991	0.9982
Weber and Morris model			
Ki	1.0449	1.1209	1.0356
c	14.452	21.275	26.569
R^2	0.9628	0.9168	0.9704

Better fit of the kinetic model is shown by higher values of the correlation coefficient (R^2) and lower values of the corresponding SSE value. The computed R^2 value of PSO was much higher than that of the PFO model as shown in Table .2.

Fig. 8 also further supports this model's superior linearity. In addition, the equilibrium capacity values

q_e that were theoretically predicted using the PSO model fit were nearer to the experimental values. As a result, it has been demonstrated that MG adsorption on NC: GO followed PSO adsorption kinetics.
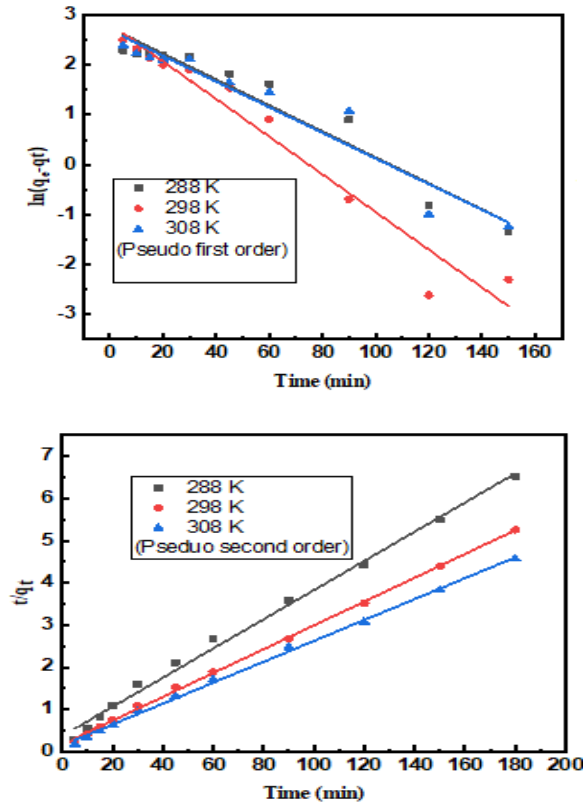

Figure 8. Kinetic models for the adsorption of MG dye onto the adsorbent NC: GO nanocomposite Pseudo-first-order and Pseudo-second-order.

Intraparticle Diffusion Model (ID)

To highlight the rate-limiting step, the Webber–Morris model (ID) was applied Eq. 6.

$$q_t = k_i\sqrt{t} + C \qquad \ldots\ldots\ldots\ldots\ldots 6$$

From the plot amount adsorbed at t time (q_t) against the square root of contact time ($\sqrt{t}$) , the intra-particle diffusion rate constant k_i (mg/g.min$^{-1/2}$) and C (mg/g) is estimated from the slope and intercept respectively see Table 2. The values of C are related to the thickness of the boundary layer. The larger C implies a greater effect on the boundary layer. As shown in Fig. 9, three steps were detected in the whole adsorption process: the initial fragment was ascribed to external diffusion and the second fragment was attributed to intraparticle diffusion, the third fragment may be due to diffusion of the adsorbate MG through smaller pores of adsorbent then followed by the equilibrium due to the low

solute concentration of MG in solution. From Fig. 9, we can also observe the straight line fitted didn't go through the origin sign that the intra-particle diffusion was not the only rate-controlling step[33].
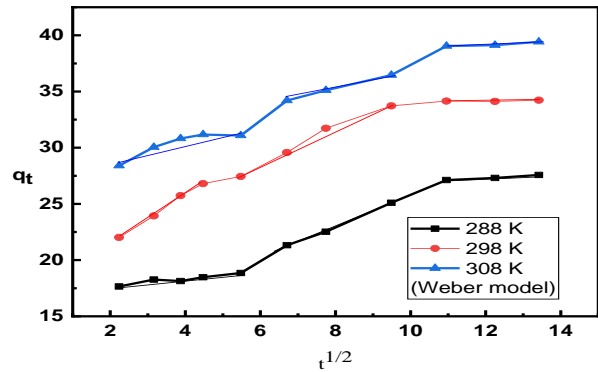

Figure 9. Kinetic plot of intra-particle diffusion model

To determine the true rate-controlling step for the adsorption of MG on CN: GO adsorbent Boyd equation[34] has been used to analyze kinetic data. It is presented as the following

$$-\ln(1-F) = k_b t \qquad \ldots\ldots\ldots\ldots\ldots 7$$

Where k_b is Boyd constant (min^{-1}) and F is the fractional attainment of equilibrium can be defined by q_t/q_e. Fig. 10 shows that there is a linear pattern with no zero intercept value, demonstrating the significance of both film diffusion and pore diffusion as regulatory processes for the MG mechanism adsorption on NC: GO [35,36].
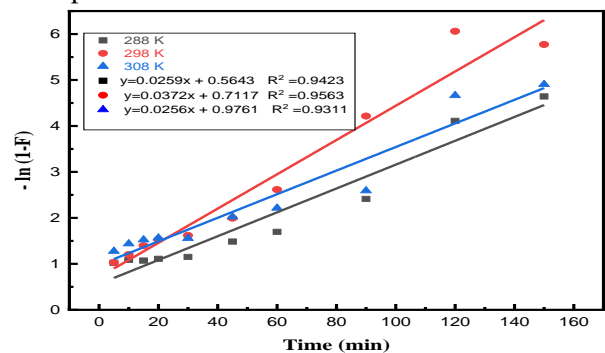

Figure 10. Boyd plot for MG adsorption onto NC: GO adsorbent

Adsorption Isotherms

The MG adsorption isotherms on NC: GO adsorbent at 288, 298, and 308 K are shown in Fig. 11 and demonstrate that the equilibrium uptake increased as the concentration of MG increased; this might be because there were more MG ions nearby the NC: GO active sites. The fact that the equilibrium adsorption increased with temperature further

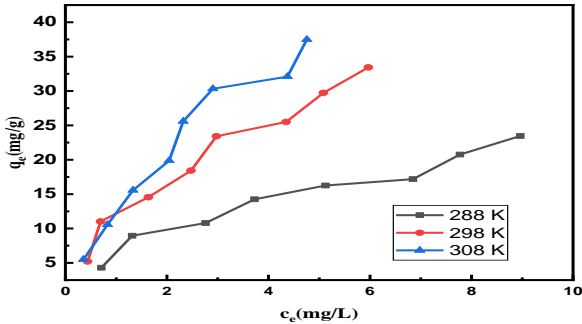supports the endothermic nature of the MG adsorption on NC: GO adsorbent.

Figure 11. The effect of temperature on NC: GO ability to adsorb MG dye

The experimental data are generally shown graphically to further explain the interaction between the adsorbate and the adsorbent at a constant temperature. Langmuir and Freundlich's models were used to simulate the data from adsorption isotherms. Langmuir 1916 provided a model for chemical adsorption (chemisorption) [37]. The following expression gives the Langmuir equation's linearized form.

$$\frac{c_e}{q_e} = \frac{1}{q_{max}.k_L} + \frac{c_e}{q_{max}} \qquad ……………..8$$

A plot of c_e/q_e versus c_e yields a straight line. The slope can be identified with the amount of MG dye needed to form a monolayer on the surface of NC: GO (q_{max} in mg/g) and the intercept with a constant affinity of the adsorption sites (k_L in L/mg). According to Hall et al [38], the essential characteristics of a Langmuir isotherm can be stated in terms of a dimensionless constant separation factor which is determined using the following equation [37].

$$R_L = \frac{1}{1+K_L c_o} \qquad ……………9$$

Where c_o (mg/L) is the maximum MG dye concentration and K_L (L/mg) is the Langmuir constant. Table 3 includes the calculated values of R_L at 288, 298, and 308 K. The current adsorption process is favorable because the R_L values range from 0 to 1[38–40]. An acceptable isotherm that can be utilized for adsorption from solution is the empirical isotherm of Freundlich. The Freundlich isotherm is the type of isotherm that is most appropriate for explaining electrostatic attraction, H-bonding and π-π interaction. The convenient way to write the logarithmic form is as follows:

$$\ln q_e = \ln k_f + \frac{1}{n}\ln c_e \qquad …………..10$$

Where K_f and n are the capacity adsorption, and intensity of adsorption respectively. The constants K_f and n can be concluded from the intercept and slope of the plot ln qe versus ln c_e. Table 3 summarizes the parameters and R^2 of Langmuir and Freundlich adsorption isotherms. Comparison of the correlation coefficients of Langmuir and Freundlich equations demonstrates that the Freundlich equation fits MG adsorption better than Langmuir. The n values higher than 1 indicate that the adsorption process on NC: GO adsorbent is physical and has a high degree of heterogeneity [41,42].

Table 3. Isotherm parameters and correlation coefficients for the adsorption of MG on NC: GO at different temperatures.

Isotherms	Parameters	Temperatures		
		288 K	**298 K**	**308 K**
Langmuir	K_L(L/mg)	0.21	0.2808	0.2260
	q_{max} (mg/g)	32.67	50.00	69.44
	R_L	0.22	0.18	0.21
	R^2	0.9132	0.9145	0.9049
Freundlich	K_f (mg/g)/ mg/L)^n	6.18	10.77	12.26
	n	1.69	1.58	1.36
	R^2	0.9580	0.9545	0.9836

Thermodynamic Analysis

To demonstrate how temperature affects the adsorption process of the MG dye on the NC: GO adsorbent, the standard entropy change ($\Delta S°$), enthalpy change ($\Delta H°$), and free energy change ($\Delta G°$) were determined. The standard Gibbs energy change of the adsorption process can be calculated from the constant of the standard thermodynamic equilibrium ($K_{eq}°$) according to Eq. 11

$$\Delta G° = -RT \ln K_{eq}° \qquad ……………..11$$

Where R is the universal gas constant 8.314 J/mole .K and T absolute temperature (K). By graphing ln q_e/c_e vs q_e and extrapolating q_e to zero it is possible to determine the values of $K_{eq}°$ (L/g) [43] as illustrated in Fig. 12.
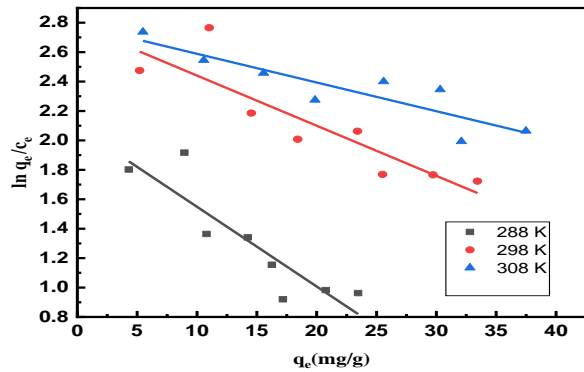
Figure 12. Plots of ln (q_e/c_e) versus qe for adsorption of MG on NC: GO adsorbent.

At a given temperature the $\Delta G°$ can be deduced in term of the change in $\Delta S°$ and $\Delta H°$ according to Eq. 12 below

$$\Delta G° = \Delta H° - T\Delta S° \qquad \ldots\ldots\ldots\ldots\ldots12$$

By substitution eq.12 in eq. 11 yield

$$\ln K°_{eq} = \frac{\Delta S°}{R} - \frac{\Delta H°}{RT} \qquad \ldots\ldots\ldots\ldots\ldots\ldots13$$

plotting $\ln K°_{eq}$ versus (1/T) gives a linear relationship. The slope is equal to - $\Delta H°$/R, and the intercept equal to $\Delta S°$/R. The values of $\Delta G°$, $\Delta H°$ and $\Delta S°$ are listed in Table 4. The spontaneous character $\Delta G°< 0$ and $\Delta G°< 20$ KJ/mole suggests that the molecules of MG dye are more responsive to NC: GO adsorb. The adsorption process can be categorized as an endothermic and phyisorption process based on the magnitude of $\Delta H° > 0$ and $\Delta H°$ <80 kJ/mol. Additionally, the positive $\Delta S°$ value showed that the degrees of freedom at the solid-liquid interface expanded during the adsorption process [44].

Table 4. Thermodynamic Parameters for adsorption of MG onto the NC: GO adsorbent

T/K	$\Delta G°$ (KJ/mole)	$\Delta S°$ (J/mole.K)	$\Delta H°$ (KJ/mole)	Ea (KJ/mole)
288	-5.00	107.99	25.83	9.57
298	-6.89			
308	-7.12			

Furthermore, the straight-line plot of $\ln K_2$ against 1/T Fig. 13 is used to compute the activation energy (E_a) from the slope using the Arrhenius formula as shown below

$$\ln k_2 = \ln A - \frac{E_a}{RT} \qquad \ldots\ldots\ldots\ldots..14$$

Where A and k_2 are the Arrhenius factor and the PSO rate constant respectively. The magnitude of the activation energy gives a clue as to whether the adsorption is mostly chemical or physical. Higher activation energies (40–800 kJ/mol) imply chemisorption, while lower activation energies (5–40 kJ/mol) are typical of phyisorption [43, 44]. For the MG adsorption onto NC: GO, the outcome is 32.16 kJ/mol (see Table 4), suggesting that the adsorption has a low potential barrier and corresponds to a phyisorption process [45-47].
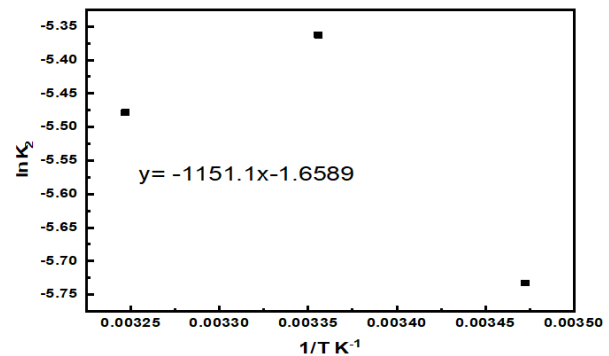

Figure 13. ln K_2 versus 1/T

Conclusion

NC: GO nanocomposite has been synthesized as adsorbent to remove MG dye from an aqueous solution by in situ deposition of nickel cobaltite on GO sheets. The XRD, SEM and FTIR analyses were used to investigate the physicochemical properties of GO, NC and NC: GO nanocomposite. XRD analysis showed a good agreement between NC characteristic peaks and JCPDS. Through this study, the optimum value of adsorbent dosage was obtained 3 mg and the contact time was 120 minutes. The equilibrium data have been examined utilizing the Langmuir and Freundlich isotherms. The isotherm's distinctive parameters and associated correlation coefficients have been identified. The Freundlich isotherm offers better correlation which means that the electrostatic interaction between the MG dye and the functional groups on the NC: GO adsorbent controls the dyes' ability to adsorb. The kinetic data were best represented by the pseudo-second order kinetic model. According to Boyd and Weber and Morris models the results indicated that both film diffusion

and intraparticle diffusion are involved in the mechanism adsorption of MG. The calculation of thermodynamic parameters revealed that the adsorption of MG is a spontaneous, a phyisorption process, and endothermic process.

Authors' Declaration

- Conflicts of Interest: None.
- We hereby confirm that all the Figures and Tables in the manuscript are ours. Besides, the Figures and Images, which are not ours, have been given the permission for re-publication attached with the manuscript.
- Ethical Clearance: The project was approved by the local ethical committee at University of Baghdad.

Authors' Contribution Statement

M. A. A. and S. H. M. contributed to the design and implementation of the research. M. A. A. prepared GO, NC and its composite and performed the analysis of the results FT-IR,XRD. M. A. A. made the adsorption experiments. S. H. M. worked on the manuscript, designed the figures, and interpreted the results.

References

1. Lellis B, Fávaro P, Cíntia Z F P, João A P, Julio C. Effects of textile dyes on health and the environment and bioremediation potential of living organisms. Biotechnol Res Innov. 2019; 3(2): 275 290. https://doi.org/10.1016/j.biori.2019.09.001

2. Routoula E, Siddharth V P. Degradation of anthraquinone dyes from effluents: A Review Focusing on Enzymatic Dye Degradation with Industrial Potential. Environ Sci Technol. 2020; 54(2): 647 664. https://doi.org/10.1021/acs.est.9b03737

3. Sun Sh, Yao H, Fu W, Xue Sh, Zhang W. Enhanced degradation of antibiotics by photo-fenton reactive membrane filtration. J Hazard Mater. 2020; 386(2019): 121955. https://doi.org/10.1016/j.jhazmat.2019.121955

4. Khettaf S, Boumaraf R, Benmahdi F, Bouhidel KE, Bouhelassa M. Removal of the neutral dissolved organic matter (NDOM) from surface water by coagulation/flocculation and nanofiltration. Anal Lett. 2021; 54(17): 2713–26. https://doi.org/10.1080/00032719.2021.1885040

5. Abid MF, Zablouk MA, Abid-Alameer AM. Experimental study of dye removal from industrial wastewater by membrane technologies of reverse osmosis and nanofiltration. Iran J Environ Heal Sci Eng. 2012; 9(17): 1. https://doi.org/10.1186/1735-2746-9-17

6. Bustos-Terrones YA, Hermosillo-Nevárez JJ, Ramírez-Pereda B, Vaca M, Rangel-Peraza JG, Bustos-Terrones V, et al. Removal of BB9 textile dye by biological, physical, chemical, and electrochemical treatments. J Taiwan Inst Chem Eng. 2021; 121: 29–37 10. https://doi.org/10.1016/j.jtice.2021.03.041

7. Imranullah M, Hussain T, Ahmad R, Hwang JS, Ahmad S, Shakir I, et al. Hierarchical porous spinel nickel cobaltite nanoflakes anchored reduced graphene oxide nano-photocatalyst for efficient degradation of organic pollutants under natural sunlight. J Mater Res Technol. 2021; 15: 623–32. https://doi.org/10.1016/j.jmrt.2021.08.030

8. Das R, Vecitis CD, Schulze A, Cao B, Ismail AF, Lu X, et al. Recent advances in nanomaterials for water protection and monitoring. Chem Soc Rev. 2017; 46(22): 6946–7020. http://dx.doi.org/10.1039/c6cs00921b

9. Talbot D, Queiros Campos J, Checa-Fernandez BL, Marins JA, Lomenech C, Hurel C, et al. Adsorption of organic dyes on magnetic iron oxide nanoparticles. Part I: Mechanisms and adsorption-induced nanoparticle agglomeration. ACS Omega. 2021; 6(29): 19086–98. https://doi.org/10.1021/acsomega.1c02401

10. Mohanta J, Dey B, Dey S. Magnetic Cobalt Oxide Nanoparticles: Sucrose-assisted self-sustained combustion synthesis, characterization, and efficient removal of malachite green from water. J Chem Eng Data. 2020; 65(5): 2819–29. https://doi.org/10.1021/acs.jced.0c00131

11. Hosny N M, Gomaa I A, Anwar Z M. Synthesis, magnetic and adsorption of dye onto the surface of NiO nanoparticles. J Mater Sci Mater Electron.2020; 31(11): 8413 8422. https://doi.org/10.1007/s10854-020-03376-w

12. Zhou P, An J, Wen X. Facile synthesis and highly efficient Congo red adsorption of a novel hierarchical ZnO nanorod/NiCo2O4 nanosheet composite nanomaterials. Mater Res Express. 2019; 6(12): 1-10.

13. Das T R, Sharma P K. Bimetal oxide decorated graphene oxide (Gd2O3/Bi2O3@GO) nanocomposite as an excellent adsorbent in the removal of methyl orange dye. Mater Sci Semicond Process. 2020; 105(August 2019): 104721. https://doi.org/10.1016/j.mssp.2019.104721

14. The Ky V, Trinh T Ph, Nguyen V C, Kim J. Facile synthesis of graphite oxide/MIL-101(Cr) hybrid composites for enhanced adsorption performance towards industrial toxic dyes. J Ind Eng Chem. 2021; 95: 224 234. https://doi.org/10.1016/j.jiec.2020.12.023

15. Adel M, Ahmed M A, Mohamed A A. A facile and rapid removal of cationic dyes using hierarchically porous reduced graphene oxide decorated with manganese ferrite. Flat Chem. 2021; 26(January): 100233. https://doi.org/10.1016/j.flatc.2021.100233

16. Mao B, Sidhureddy B, Thiruppathi AR, Wood PC, Chen A. Efficient dye removal and separation based on graphene oxide nanomaterials. New J Chem. 2020; 44(11): 4519–28. https://doi.org/10.1039/c9nj05895h

17. Suhaimin N S, Hanifah, Mohamad F R, Jusin J w, Jaafar J, Aziz M, Ismail A F, et al. Tuning the oxygen functional groups in graphene oxide nanosheets by optimizing the oxidation time. Physica E Low Dimens. Syst. Nanostruct .2021; 131(2020): 114727.https://doi.org/10.1016/j.physe.2021.114727

18. Tarighi S, Juibari NM. Green synthesized manganese-cobaltite nanospinel and its dye removal characteristics: isothermal and kinetic studies. ChemistrySelect. 2019; 4(21): 6506–15. https://doi.org/10.1002/slct.201900816

19. Ibrahim SM, Badawy AA, Essawy HA. Improvement of dyes removal from aqueous solution by Nanosized cobalt ferrite treated with humic acid during coprecipitation. J Nanostructure Chem. 2019; 9(4): 281–98. https://doi.org/10.1007/s40097-019-00318-9

20. Chen H, Zheng Y, Cheng B, Yu J, Jiang C. Chestnut husk-like nickel cobaltite hollow microspheres for the adsorption of Congo red. J Alloys Compd. 2018; 735: 1041–51. https://doi.org/10.1016/j.jallcom.2017.11.192

21. Hummers WS, Offeman RE. Preparation of Graphitic Oxide. J Am Chem Soc. 1958; 80(6): 1339. https://doi.org/10.1021/ja01539a017

22. Chen X, Qu Z, Liu Z, Ren G. Mechanism of oxidization of graphite to graphene oxide by the Hummers method. ACS Omega. 2022; 7(27): 23503 23510. https://doi.org/10.1021/acsomega.2c01963

23. Park H, Park B H, Choi J, Kim S, Taesung K, Youn Y S, et al. Enhanced electrochemical properties and oer performances by cu substitution in nico2 o4 spinel structure. Nanomaterials. 2020; 10(9): 1 19. https://doi.org/10.3390/nano10091727

24. Khalid S, Cao C, Wang L, Zhu Y. Microwave assisted synthesis of porous NiCo2O4 microspheres: Application as high performance asymmetric and symmetric supercapacitors with large areal capacitance. Sci Rep. 2016; 6(March): 1-13. https://dx.doi.org/10.1038/srep22699

25. Merza SH, Mousa EF. Dielectric properties of ultra-low dielectric constant PVA-pentaerythritol/MnO2 nanocomposite. Phys Chem Res. 2022; 10(3): 325–31.

26. Díez-pascual AM, Sainz-urruela C, Vallés C, Vera-lópez S, Andrés MPS. Tailorable synthesis of highly oxidized graphene oxides via an environmentally-friendly electrochemical process. Nanomaterials. 2020; 10(2): 1–18. https://doi.org/10.3390/nano10020239

27. Elbasuney Sh, El-Sayyad Gh S, Yehia M, Abdel Aal S K.. Facile synthesis of RGO-Fe2O3 nanocomposite: A novel catalyzing agent for composite propellants. J Mater Sci Mater Electron. 2020; 31(23): 20805-20815. https://doi.org/10.1007/s10854-020-04593-z

28. Coates J. Interpretation of Infrared Spectra, A Practical Approach. Encycl Anal Chem. 2006; 1–23. https://doi.org/10.1002/9780470027318.a5606

29. Haripriya M, Sivasubramanian R, Ashok AM, Hussain S, Amarendra G. Hydrothermal synthesis of NiCo2O4 –NiO nanorods for high performance supercapacitors. J Mater Sci Mater Electron. 2019; 30(8): 7497–7506. https://dx.doi.org/10.1007/s10854-019-01063-z

30. Wang Y, Liu X, Wang H, Xia G, Huang W, Song R. Microporous spongy chitosan monoliths doped with graphene oxide as highly effective adsorbent for methyl orange and copper nitrate (Cu(NO3)2) ions. J Colloid Interface Sci. 2014; 416: 243–51. https://dx.doi.org/10.1016/j.jcis.2013.11.012

31. Barbooti M M, Zahraw S H. Removal of amoxicillin from water by adsorption on water treatment residues. Baghdad Sci J. 2020; 17(3): 1071- 1079. https://doi.org/10.21123/bsj.2020.17.3(Suppl.).1071

32. Zbair M, El Hadrami Ab, Bellarbi A, Monkade M, Zradba Ab, Brahmi R. Herbicide diuron removal from aqueous solution by bottom ash: Kinetics, isotherm, and thermodynamic adsorption studies. J Environ Chem Eng. 2020; 8(2), 103667. https://doi.org/10.1016/j.jece.2020.103667

33. Ahmadi A, Foroutan R, Esmaeili H, Tamjidi S. The role of bentonite clay and bentonite clay@MnFe2O4 composite and their physico-chemical properties on the removal of Cr(III) and Cr(VI) from aqueous

media. Environ Sci Pollut Res. 2020; 27(12): 14044 14057.https://doi.org/10.1007/s11356-020-07756-x

34. Lin D, Wu F, Hu Y, Zhang T, Liu Ch, Hu Q, et al. Adsorption of dye by waste black tea powder: parameters, kinetic, equilibrium, and thermodynamic studies. J Chem. 2020; 2020: 13. https://doi.org/10.1155/2020/5431046

35. Akbarnejad S, Amooey AA, Ghasemi S. High effective adsorption of acid fuchsin dye using magnetic biodegradable polymer-based nanocomposite from aqueous solutions. Microchem J . 2019; 149(May): 1–12. https://doi.org/10.1016/j.microc.2019.103966

36. Jain SN, Sonawane DD, Shaikh ER, Garud VB, Dawange SD. Vegetable residue of fenugreek (Trigonella Foenum-Graecum), waste biomass for removal of Basic Violet 14 from wastewater: Kinetic, equilibrium, and reusability studies. Sustain Chem Pharm. 2020; 16:1–9. https://doi.org/10.1016/j.scp.2020.100269

37. Lafi R, Imed M, Hafiane A. Adsorption of congo red dye from aqueous solutions by prepared activated carbon with oxygen-containing functional groups and its regeneration. Adsorp Sci Technol. 2019; 37(1 2): 160 181. https://doi.org/10.1177/0263617418819227

38. Hall KR, Eagleton LC, Acrivos A, Vermeulen T. Pore- and solid-diffusion kinetics in Fixed-Bed Adsorption Under Constant- Pattern Conditions. Ind Eng 52212, Chem Fundam. 1996; 5(2): 212–23. https://doi.org/10.1021/i160018a011

39. Tang Sh H, Ahmad Z, Muhammad A. Development of activated carbon pellets using a facile low-cost binder for effective malachite green dye removal. J Clean Prod. 2020; 253: 119970. https://doi.org/10.1016/j.jclepro.2020.119970

40. Alardhi S M, Alrubaye J M, Albayati T M. Adsorption of methyl green dye onto MCM-41: Equilibrium, kinetics and thermodynamic studies. desalin water treat. 2020; 179: 323 331. https://doi.org/10.5004/dwt.2020.25000

41. Hicham A, Hussein J, Siba H. Kinetic, isotherm and thermodynamic studies on the ciprofloxacin adsorption from aqueous solution using Aleppo bentonite. Baghdad Sci J. 2022; 19(3): 680–92. https://doi.org/10.21123/BSJ.2022.19.3.0680

42. Sharafinia S, Farrokhnia A, Lemraski EG. Comparative study of adsorption of safranin o by TiO2/activated carbon and chitosan/TiO2/activated carbon adsorbents. Phys Chem Res. 2021; 9(4): 605–21. https://doi.org/10.22036/PCR.2021.274568.1889

43. Günay A, Arslankaya E, Tosun I. Lead removal from aqueous solution by natural and pretreated clinoptilolite: Adsorption equilibrium and kinetics. J Hazard Mater. 2007; 146(1–2): 362–71. https://doi.org/10.1016/j.jhazmat.2006.12.034

44. Rida K, Chaibeddra K, Cheraitia K. Adsorption of cationic dye methyl green from aqueous solution onto activated carbon prepared from brachychitonpopulneus fruit shell. Indian J Chem Technol. 2020; 27(1): 51–9. https://doi.org/10.56042/ijct.v27i1.22949

45. Bai W, Qian M, Li Q, Atkinson S, Tang B, Zhu Y, et al. Rice husk-based adsorbents for removing ammonia: Kinetics, thermodynamics and adsorption mechanism. J Environ Chem Eng. 2021; 9(4): 105793. https://doi.org/10.1016/j.jece.2021.105793

46. Esfandiari N, Kashefi M, Mirjalili M, Afsharnezhad S. Role of silica mid-layer in thermal and chemical stability of hierarchical Fe3O4-SiO2-TiO2 nanoparticles for improvement of lead adsorption: Kinetics, thermodynamic and deep XPS investigation. Mater Sci Eng B: Solid State Mater Adv Technol. 2020; 262(August): 114690. https://doi.org/10.1016/j.mseb.2020.114690

47. Abbas AM, Abd SS, Himdan T AB. Kinetic study of methyl green dye adsorption from aqueous solution by bauxite clay at different temperatures. Ibn AL-Haitham J Pure Appl Sci. 2018; 31(1): 58–66. https://doi.org/10.30526/31.1.1853

تزيين أوكسيد الجرافين بدقائق كوبلتيت النيكل النانوية كسطح ماز لصبغة الميثيل الأخضر الكاتيونية: دراسات حركية ، ايزوثيرمية ، وديناميكية حرارية

مريم عبد الهادي عبد الستار، سندس هادي مرزا

قسم الكيمياء، كلية التربية للعلوم الصرفة (ابن الهيثم)، جامعة بغداد، بغداد، العراق.

الخلاصة

تم في هذه الدراسة ، تزيين رقائق أكسيد الجرافين (GO) بجسيمات كوبلتيت النيكل النانوية $NiCo_2O_4$ (NC) عن طريق الترسيب في الموقع ، وتم استخدام المتراكب المحضر (NC: GO) كسطح ماز لإزالة صبغة الميثيل الخضراء (MG) من المحاليل المائية. تم التحقق من التغطية الناجحة لأوكسيد الجرافين بجزيئات كوبلتيت النيكل النانوية (NC) باستخدام دراسات FT-IR وحيود الأشعة السينية (XRD). كانت أحجام الجسيمات البلورية لل NC و لل GO المزين ب NC هي 10.53 نانوميتر و 9.30 نانومتر على التوالي. تم دراسة تأثير العديد من العوامل التجريبية ، بما في ذلك زمن التلامس ، وكمية السطح الماز ، ودرجة الحرارة. كان وقت التلامس الأمثل وكمية السطح 120 دقيقة و 3 مجم / لتر على التوالي. تتلائم بيانات الامتزاز بشكل أفضل مع ايزوثيرم Freundlich. تم استخدام أربعة نماذج حركية لتتبع عملية الامتزاز: معادلة زائفة من الدرجة الأولى ، ومعادلة زائفة من الدرجة الثانية ، ومعادلة الانتشار داخل الجسيمات ، ومعادلة بويد. أظهرت نمذجة البيانات التجريبية أن حركية الامتزاز كانت ممثلة بشكل جيد بنموذج الرتبة الثانية الزائفة ($R^2 = 0.9945$) مع معدل ثابت يبلغ 3.2×10^{-3} (جم / مجم. دقيقة). يتم امتصاص صبغة MG تدريجيًا بواسطة الجسيمات النانوية NC من خلال الانتشار داخل الجسيمات ويتم الاحتفاظ بها بعد ذلك في مسام أصغر. أظهرت قيم التحليل الديناميكي الحراري أن عملية امتزاز صبغة MG كانت ماصة للحرارة بطبيعتها ، و تلقائية وعملية الامتزاز فيزيائية.

الكلمات المفتاحية: معادلة بويد، معادلة ديباي شرر، الانتشار داخل الجسيمات ، المسافات البينية، النموذج الزائف من الدرجة الأولى.